28

Multiobjective Design Exploration in Space Engineering

Akira Oyama and Kozo Fujii
Institute of Space and Astronautical Science, Japan Aerospace Exploration Agency
Japan

1. Introduction

Most of real world design optimization problems in space engineering are multiobjective design optimization problems that simultaneously involve several competing objectives (Oyama et al., 2002) (Tani et al., 2008) (Oyama et al., 2009) (Oyama et al., 2010). For example, design of a turbopump for liquid rocket engine involves maximization of total head, minimization of input power, minimization of weight, minimization of manufacturing cost, and so on. Another example is trajectory design of a spacecraft where payload weight should be maximized, time required to reach the target point should be minimized, distance from the sun should be maximized (or minimized), and manufacturing cost should be minimized. Many other multiobjective design optimization problems can be easily found, such as reusable space transportation system design, spacecraft design, and Mars airplane design.

While a single objective design optimization problem may have a unique optimal solution, multiobjective design optimization problems present a set of compromised solutions, largely known as Pareto-optimal solutions or non-dominated solutions. Each of these solutions is optimal in the sense that no other solutions in the search space are superior to it when all objectives are considered (Fig. 1). Therefore, the goal of multiobjective design optimization problems is to find as many non-dominated solutions as possible to provide useful information of the problem to the designers.

Recently, idea of multiobjective design exploration (MODE) (Obayashi et al., 2005) is proposed as a framework to extract essential knowledge of a multiobjective design optimization problem such as trade-off information between contradicting objectives and the effect of each design parameter on the objectives. In the framework of MODE, non-dominated solutions are obtained by multiobjective optimization using, for example, a multiobjective evolutionary computation (Deb, 2001), and then design knowledge is extracted by analysing the values of objective functions and design parameters of the obtained non-dominated solutions. There, data mining approaches such as the self-organizing map (SOM) (Kohonen, 1998) and analysis of variance (ANOVA) (Donald, 1998) are used. Recently, MODE framework has been applied to a wide variety of design optimization problems including multidisciplinary design of a regional-jet wing (Chiba et al., 2007a) (Chiba et al., 2007b), aerodynamic design of multi-element airfoil (Kanazaki et al., 2007), and car tire design (Shimoyama, 2009).

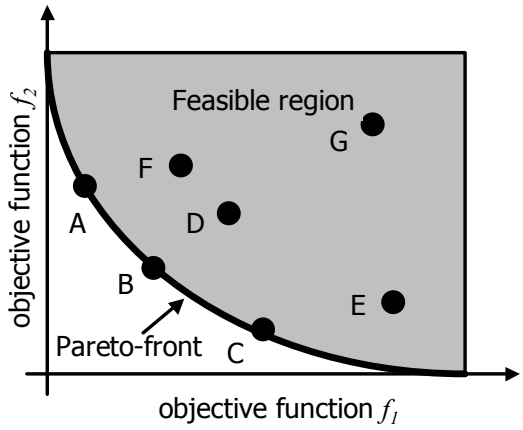

Fig. 1. The concept of Pareto-optimality. This is an example of multiobjective design optimization problems, which minimizes two conflicting objectives f_1 and f_2. Gray-colored area is feasible region where solutions can exit. This problem has innumerable compromised non-dominated solutions such as solutions A, B, and C on the edge of the feasible region (Pareto-front). These solutions are optimal in the sense that there is no better solution in both objectives. One cannot say which is better among these non-dominated solutions because improvement in one objective degrades another.

Although the MODE framework is useful for real-world designs, analysis of design parameters and objective functions values of the non-dominated solutions is not sufficient for design exploration in space engineering. For example, for a wing shape design optimization problem, design knowledge one can obtain depends on how the shape is parameterized. If an airfoil (i.e., wing profile) shape is represented by B-spline curves and the coordinates of the B-spline curves are considered as the design parameters, it is difficult to obtain design knowledge related to leading edge radius, maximum thickness, or trailing edge angle (Fig. 2). Another reason is that data mining of the objective function and design parameter values does not lead to understanding of the physics behind the design problem. For example, if only the design parameter and objective function values of non-dominated airfoils were analysed, it would not be possible to clarify the relation between shock wave generation and aerodynamic characteristics of an airfoil.

To solve such problems, it is necessary to analyse shape data and flow data of the obtained non-dominated solutions. Fortunately, in the process of objective function value evaluation for aerodynamic optimization, such data is computed for each design candidate. For example, in an aerodynamic airfoil shape optimization, evaluation of objective function values requires 1) shape construction from the design parameter values, 2) computational grid generation around the shape, 3) flow computation using computational fluid dynamics, and 4) surface pressure and friction distribution on the shape (Fig.3). Therefore, analysis of the shape and flow data does not require any additional computation. What we should do is not to discard such data for data mining process after the optimization.

However, analysis of shape and flow data is not straightforward because the data set can be very large. The number of the obtained non-dominated solutions is typically 100-10,000 while each non-dominated solution has large data set (Table.1). Therefore, traditional approach such as analysis with SOM or ANOVA is not adequate any more.

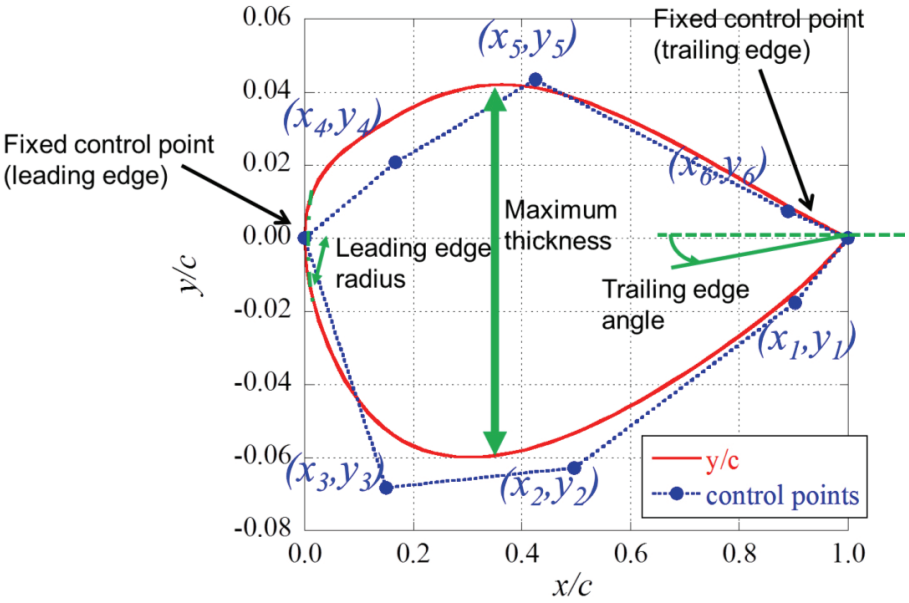

Fig. 2. An example of airfoil shape parameterization

Type of data	Typical data set size that each non-dominated solution has
two-dimensional shape data (such as airfoil)	200-2,000 (x-y coordinates of 100 to 1000 points that define the shape)
three-dimensional shape data (such as wing)	30,000-300,000 (x-y-z coordinates of 10,000 to 100,000 points that define the shape)
Two-dimensional flow data	10,000-100,000(several types of flow property (density, velocity, pressure, etc.) at the points distributed in the x-y space)
Three-dimensional flow data	500,000-5,000,000(several types of flow property (density, velocity, pressure, etc.) at the points distributed in the x-y-y space)

Table 1. Typical data set size that each non-dominated solutions has for an aerodynamic design

This chapter introduces a new approach that enables analysis of large data such set as the shape and flow data of all non-dominated solutions. This approach bases on proper orthogonal decomposition, which decomposes large data into principal modes and eigenvectors. Feasibility of this method is shown though knowledge extraction from principal modes and eigenvectors of the shape data and flow data of non-dominated solutions of an aerodynamic transonic airfoil shape optimization problem.

In section 3, characteristics of the non-dominated solutions are shown. Section 4 presents the POD-based data mining approach for analysis of non-dominated solutions. In section 5, an

application for analysis of airfoil shape data of the non-dominated solutions is presented. In section 6, flow data of the non-dominated solutions is analysed with POD.

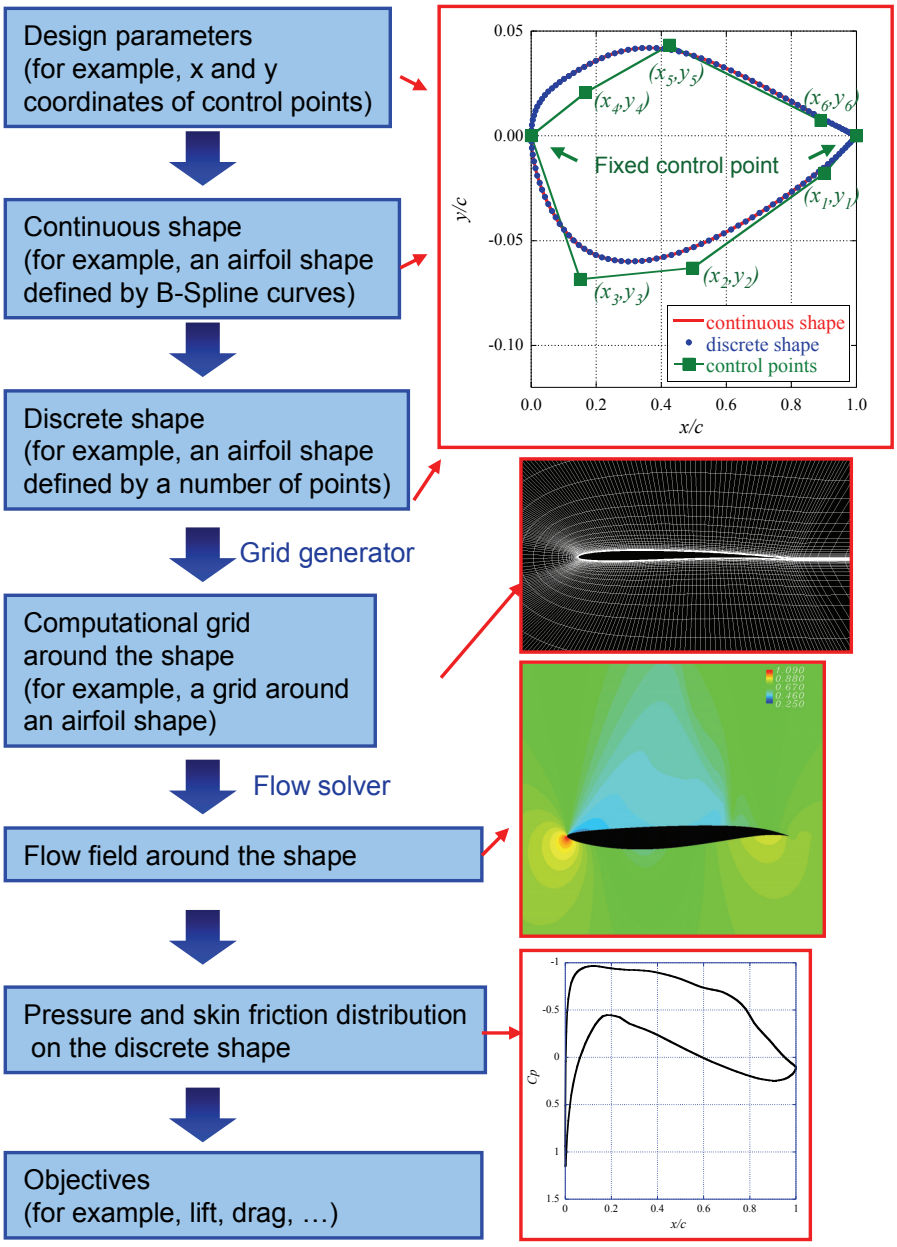

Fig. 3. Objective function value evaluation process for aerodynamic airfoil design optimization problem

2. Nomenclature

$a_m(n)$ = eigenvector of mode m of non-dominated solution n
c = airfoil chord length
C_d = drag coefficient
C_l = lift coefficient
j = index of grid points
$jmax$ = number of grid points
l/d = lift-to-drag ratio ($=C_l/C_d$)
m = index of modes
$mmax$ = number of modes ($mmax=nmax$)
n = index of non-dominated solutions
$nmax$ = number of non-dominated solutions
$p(j,n)$ = pressure of non-dominated solution n at grid point j
$q(j,n)$ = data of non-dominated solution n at grid point j
$q_{l/d\_max}(j)$ = data of maximum-lift-to-drag-ratio design at grid point j
$q'(j,n)$ = fluctuation of data $q(j,n)$ of non-dominated solution n at grid point j
$q'_{base}(j,m)$ = orthogonal base vector of mode m
$S_{m1,m2}$ = covariance of orthogonal base vectors of mode $m1$ and mode $m2$
$x(j,n)$ = coordinate in chordwise direction of non-dominated solution n at grid point j
$y(j,n)$ = coordinate in normal direction of non-dominated solution n at grid point j

3. Non-dominated solutions

The non-dominated solutions of the design optimization problem below are considered.

Objective functions:	lift coefficient (maximization)
	drag coefficient (minimization)
Constraints:	lift coefficient must be greater than 0
	maximum thickness must be greater than 0.10 chord length
Design parameters:	coordinates of 6 control points of the B-Spline curves representing an airfoil shape (Fig. 4)
Flow conditions:	free stream Mach number of 0.8
	Reynolds number of 10^6 (based on the chord length)
	angle of attack of 2 degrees.

The non-dominated solutions are obtained by a multiobjective evolutionary algorithm (MOEA) used in (Oyama et al., 2009). The present MOEA adopts real number coding, which enables efficient search in real number optimizations compared with binary or gray coding. The population size is maintained at 64 and the maximum number of generations is set to 60. The initial population is generated randomly so that the initial population covers the entire design space presented in Table 2. The fitness of each design candidate is computed according to Pareto-ranking, fitness sharing, and Pareto-based constraint handling (Oyama et al., 2007) based on its objective function and constraint function values. Here, Fonseca and Fleming's Pareto-based ranking method (Foncesa et al., 1993) and the fitness sharing method of Goldberg and Richardson (Goldberg et al., 1987) are used for Pareto-ranking where each individual is assigned a rank according to the number of individuals dominating it. In Pareto-based constraint handling, the rank of feasible designs is determined by the Pareto-ranking based on the objective function values, whereas the rank

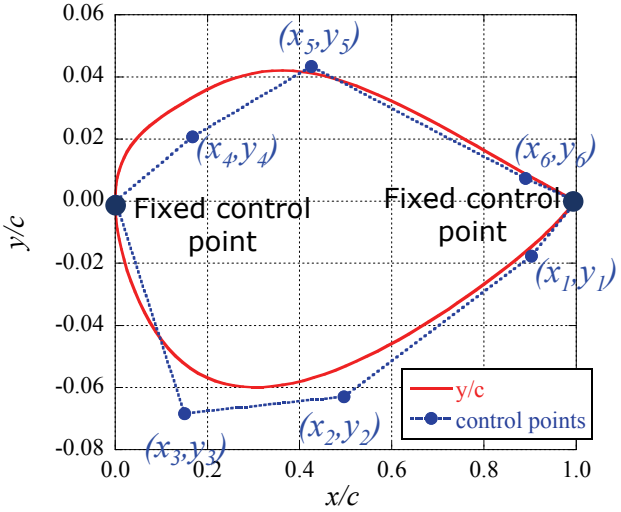

Fig. 4. Parameterization of the airfoil shape. The coordinates of six control points of the B-Spline curves representing an airfoil shape are considered as design parameters.

Design parameter	Lower bound	Upper bound
x_1	0.66	0.99
x_2	0.33	0.66
x_3	0.01	0.33
x_4	0.01	0.33
x_5	0.33	0.66
x_6	0.66	0.99
y_1	-0.10	0.10
y_2	-0.10	0.10
y_3	-0.10	0.10
y_4	0.00	0.20
y_5	0.00	0.20
y_6	0.00	0.20

Table 2. Search range of each design parameter

of infeasible designs is determined by the Pareto-ranking based on the constraint function values. The parents of the new generation are selected through roulette selection (Goldberg, 1989) from the best 64 individuals among the present generation and the best 64 individuals in the previous generation. A new generation is reproduced through crossover and mutation operators. The term "crossover" refers to an operator that combines the genotype of the selected parents and produces new individuals with the intent of improving the fitness value of the next generation. Here, the blended crossover (Eshlman et al., 1993), where the value of α is 0.5, is used for crossover between the selected solutions. Mutation is applied to the design parameters of the new generation to maintain diversity. Here, the probability of mutation taking place is 20%; this adds a random disturbance to the

corresponding gene of up to 10% of the given range of each design parameter. Present MOEA used to find quasi-optimal solutions has been well validated (Obayashi et al., 2004) (Oyama et al., 2002).

Lift and drag coefficients of each design candidate are evaluated using a two-dimensional Reynolds-averaged Navier-Stokes solver. This code employs total variation diminishing type upwind differencing (Obayashi et al., 1994), the lower-upper symmetric Gauss-Seidel scheme (Obayashi et al., 1995), the turbulence model of Baldwin and Lomax (Baldwin et al., 1985) and the multigrid method (Brant, 1977) for the steady-state problems.

All the design candidates and non-dominated solutions are plotted in Fig. 5. The number of non-dominated solutions obtained is 85. A strong trade-off between lift maximization and drag minimization is observed. This figure also indicates that there are two groups in the obtained non-dominated solutions; low drag design group (roughly, C_l <0.75) and high lift design group (roughly, C_l > 0.75).

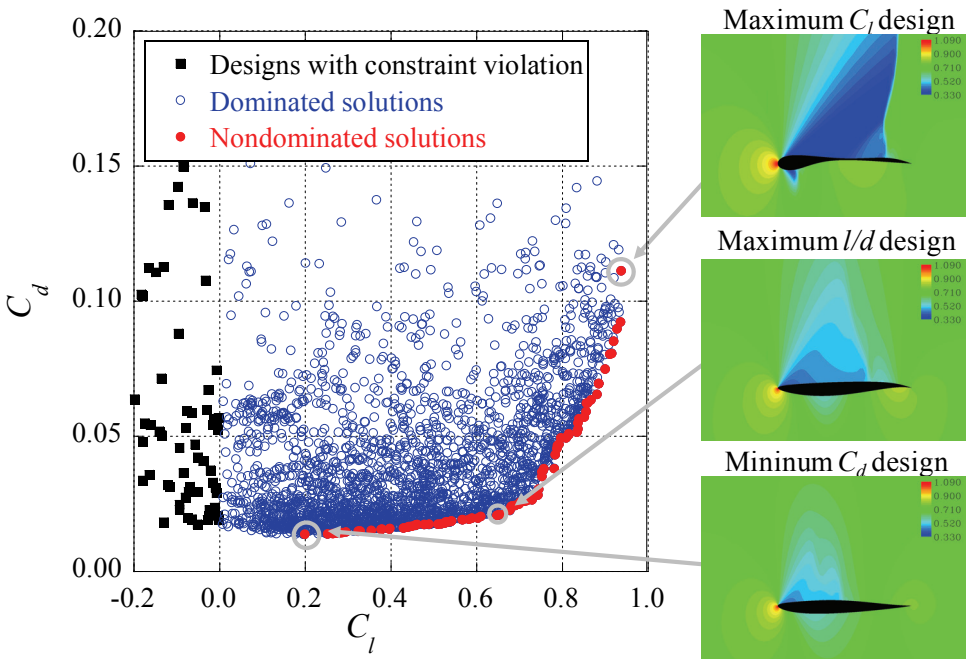

Fig. 5. Distribution of the non-dominated solutions and other design candidates with the pressure distribution around the minimum-drag, maximum-lift-to-drag-ratio, and maximum-lift airfoils.

4. Data mining approach based on POD

Proper orthogonal decomposition (POD, known as the Karhunen-Loeve expansion in pattern recognition, and principal component analysis in the statistical literature) is a statistical approach that can extract dominant features in data by decomposing the data into a set of optimal orthogonal base vectors of decreasing importance. These base vectors are

optimal in the sense that any other set of orthogonal base vectors cannot capture more information than the orthogonal base vectors obtained by POD as long as the number of base vectors is limited. The POD has also been extensively used in image processing, structural vibration, analysis of unsteady flow data and so on.

In this study, airfoil shape and flow data of the non-dominated solutions are analyzed using the snapshot POD proposed by Sirovich (Sirovich, 1987). The non-dominated solutions from the minimum drag design to the maximum-lift design are numbered as shown in Fig. 6. Each non-dominated solution has large scale data such as shape and flow defined on all grid points (Fig.7).

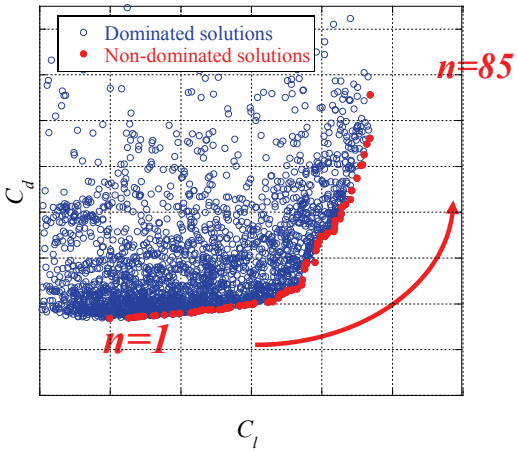

Fig. 6. Index of the non-dominated solutions. For the minimum-drag design, n=1; for the maximum-lift design, n=$nmax$=85.

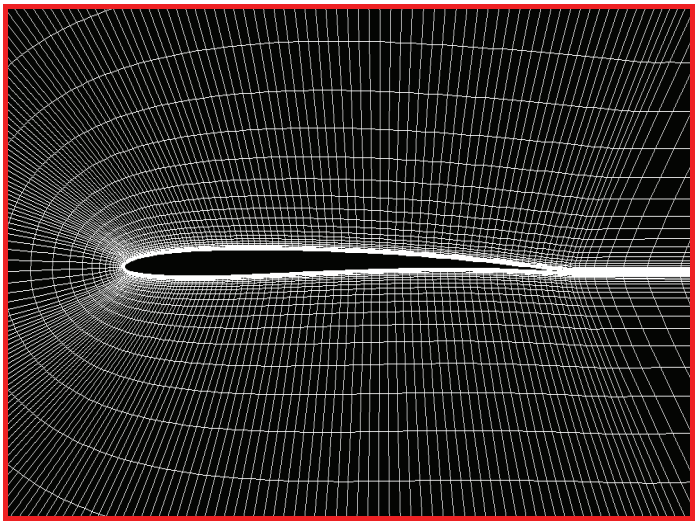

Fig. 7. Computational grid around an airfoil shape. The number of grid points is 9,849 (201x49)

In the original snapshot POD, the data to be analyzed are decomposed into the mean vector and the fluctuation vector, which is defined from the mean vector. It is known that analysis of the fluctuation from the mean vector maximizes variance of the data. However, for analysis of non-dominated solutions, it would be reasonable to define the fluctuation from one representative design, for example, the median design. Here, the fluctuation from the *l/d*-maximum design is analyzed. The data of the non-dominated solutions are decomposed into the data of the maximum-lift-to-drag-ratio design and fluctuation data as follows:

$$\begin{bmatrix} q(1,n) \\ q(2,n) \\ \vdots \\ q(j\max-1,n) \\ q(j\max,n) \end{bmatrix} = \begin{bmatrix} q_{l/d\_\max}(1) \\ q_{l/d\_\max}(2) \\ \vdots \\ q_{l/d\_\max}(j\max-1) \\ q_{l/d\_\max}(j\max) \end{bmatrix} + \begin{bmatrix} q'(1,n) \\ q'(2,n) \\ \vdots \\ q'(j\max-1,n) \\ q'(j\max,n) \end{bmatrix} \tag{1}$$

The fluctuation vector is then expressed by the linear sum of normalized eigenvectors and orthogonal base vectors as follows:

$$\begin{bmatrix} q'(1,n) \\ q'(2,n) \\ \vdots \\ q'(j\max-1,n) \\ q'(j\max,n) \end{bmatrix} = a_1(n) \begin{bmatrix} q'_{base}(1,1) \\ q'_{base}(2,1) \\ \vdots \\ q'_{base}(j\max-1,1) \\ q'_{base}(j\max,1) \end{bmatrix} + \cdots + a_{m\max}(n) \begin{bmatrix} q'_{base}(1,m\max) \\ q'_{base}(2,m\max) \\ \vdots \\ q'_{base}(j\max-1,m\max) \\ q'_{base}(j\max,m\max) \end{bmatrix} \tag{2}$$

where each eigenvector is determined so that the energy defined by Eq. (3) is maximized:

$$\sum_{j=1}^{j\max} q'^2_{base}(j,m)\,,\ m = 1, 2, \ldots, mmax \tag{3}$$

The eigenvectors that maximize the energy defined by Eq. (3) can be obtained by solving the eigenvalue problem of the following covariance matrix:

$$\begin{pmatrix} S_{1,1} & \cdots & S_{m1,1} & \cdots & S_{m\max,1} \\ \vdots & \ddots & \vdots & & \vdots \\ S_{1,m2} & \cdots & S_{m1,m2} & \cdots & S_{m\max,m2} \\ \vdots & & \vdots & \ddots & \vdots \\ S_{1,m\max} & \cdots & S_{m1,m\max} & \cdots & S_{m\max,m\max} \end{pmatrix} \tag{4}$$

where

$$S_{m1,m2} = \sum_{j=1}^{j\max} q'(j,m1)q'(j,m2) \tag{5}$$

5. Data mining of airfoil shape data

The shape data analysed here are the *y* coordinates defined on the grid points along the airfoil surface as shown in Fig. 8 where the number of grid points is 137. The energy ratios of

10 principal orthogonal base vectors (principal POD modes) to the total energy are shown in Fig. 9. While the fluctuation from the airfoil shape data of the *l/d* maximum design is analysed, principal modes are successfully extracted. The first mode is dominant (more than 83%) and the first two modes represent more than 94% of the total energy.

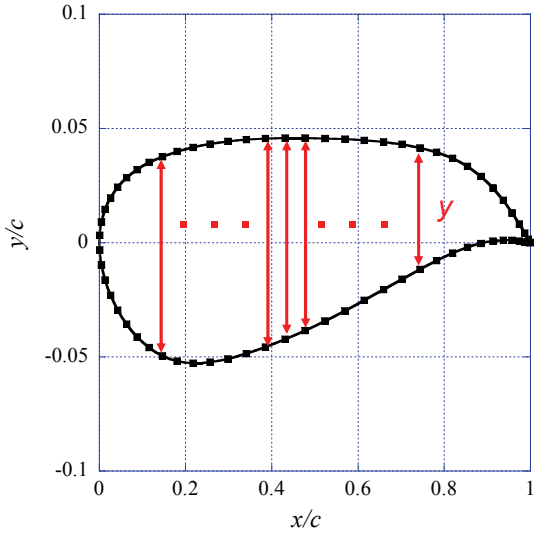

Fig. 8. Definition of the shape data. Shape data analyzed here are *y* coordinates defined on grid points along the airfoil surface.

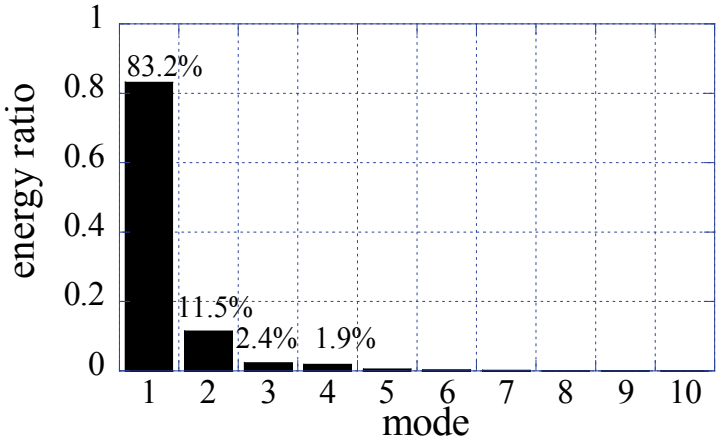

Fig. 9. Energy ratio of the top ten principal modes of the airfoil shape.

Figure 10 shows the components of the eigenvectors of the first and second modes with respect to the index of the non-dominated solutions *n* (left) and the lift coefficient $C_l(n)$ (right), respectively. Obtained non-dominated airfoil shapes are categorized into three

groups, i.e., low drag design group (roughly $1 \le n \le 39$ and $C_l < 0.65$), high l/d design group ($40 \le n \le 52$ and $0.65 < C_l < 0.75$), and high lift design group ($53 \le n \le 85$ and $C_l > 0.75$). As for the low drag design group, the second mode is dominant and the eigenvector of the first mode is approximately zero. Among the high lift design group, the first mode is dominant and the eigenvector of the second mode is small. The non-dominated solutions in the high l/d design group have no significant difference in the shape. A large jump in the first mode is observed between n=52 and n=53. This jump indicates a significant change in the shape between the high l/d designs and high lift designs.

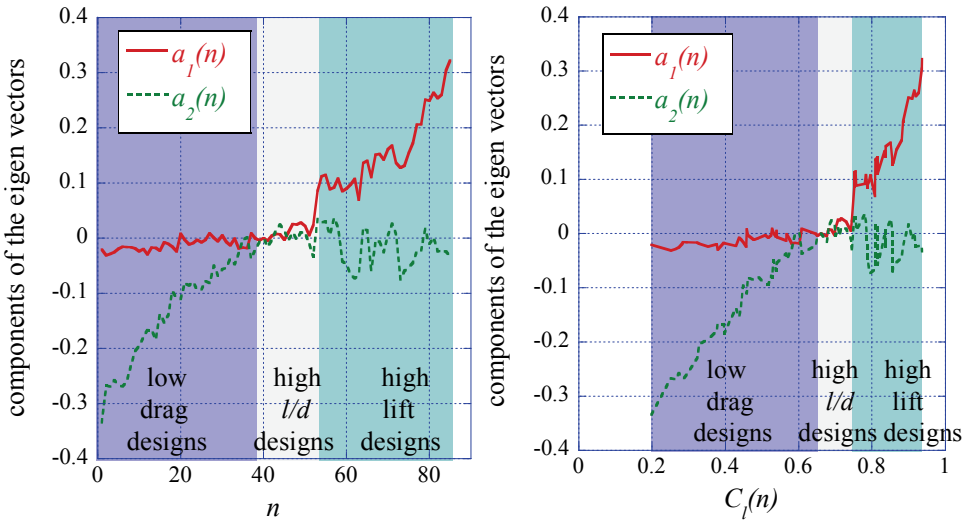

(a) Components of the eigenvectors with respect to n

(b) Components of the eigenvectors with respect to $C_l(n)$

Fig. 10. Components of the eigenvectors of the first and second modes.

Figure 11 presents the l/d-maximum airfoil shape and orthogonal base vectors of the first and second modes. This figure indicates that the mode 1 mainly contributes to the most part of the lower surface change. The base vector of the mode 1 also indicates that thickness near the leading edge should be increased as the camber is increased. This comes from the constraint on the maximum thickness imposed on the design optimization problem. The base vector of the second mode indicates that the second mode mainly contributes to the camber near the trailing edge.

Recalling the shapes of the non-dominated solutions are represented by equations (1) and (2), Figures 10 and 11 indicate that the low drag design group increase lift by changing the camber near the trailing edge while the other part of the airfoil shape is almost fixed. As for the high lift design group, lift is increased by moving the lower surface upward without significant change in the trailing edge angle. This movement of the lower surface corresponds to camber increase. The thickness near the leading edge is increased as the lower surface moves upward to satisfy the constraint applied to the airfoil maximum thickness near the leading edge.

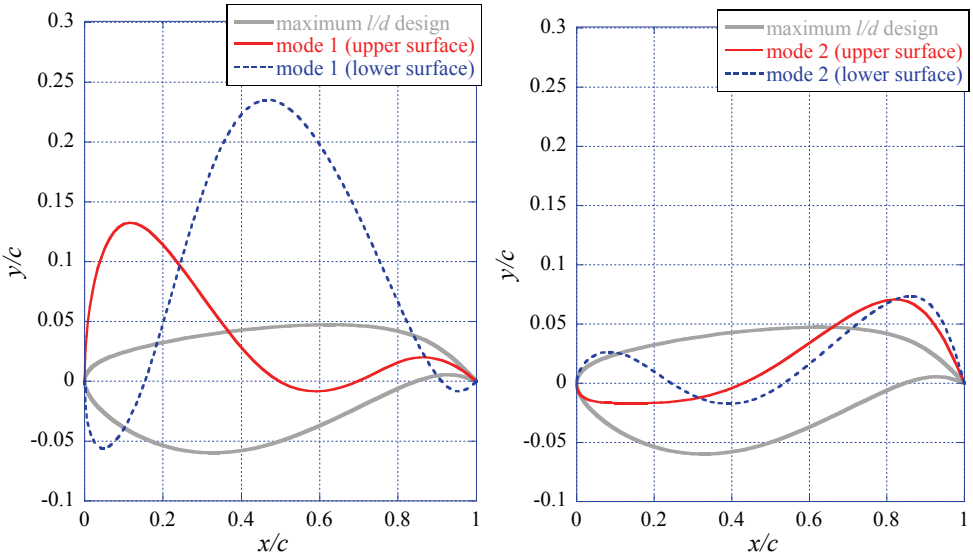

(a) Base vector of the first mode (b) Base vector of the second mode

Fig. 11. Shape of the maximum-lift-to-drag-ratio airfoil design and the orthogonal base vectors of the first and second modes.

To identify the advantage of the present approach over the conventional approach, design parameters of the non-dominated designs are analysed. Figure 12 presents scatter plots of the design parameters of the non-dominated solutions against the lift coefficient (upper) and the drag coefficient (lower). These plots give us some ideas such as 1) the non-dominated solutions may be categorized into two groups (see for example C_l against y_2 or y_4), and 2) airfoil camber increases as the lift increases. However, analysis of this figure hardly leads to the design knowledge we obtained in this section such as 1) the non-dominated solutions can be categorized into three groups, 2) Among the low drag designs, lift is increased by changing the camber near the trailing edge and 3) Among the high lift designs, the lift is increased by moving the lower surface upward. The reason for that is these features are represented by multiple design parameters. For example, camber near the trailing edge is mainly represented by x_1, y_1, x_6, and y_6.

6. Data mining of flow data

Here, as an example of flow data, static pressure data defined on all grid points of the non-dominated solutions are analysed, where the number of the grid points is 9,849 (201x49) (Fig.7). The energy ratios of the 10 principal orthogonal base vectors are presented in Fig. 13. The first mode is dominant (more than 79%) and the first two modes represent more than 92% of the total energy. These results are qualitatively the same as the airfoil shape data mining results.

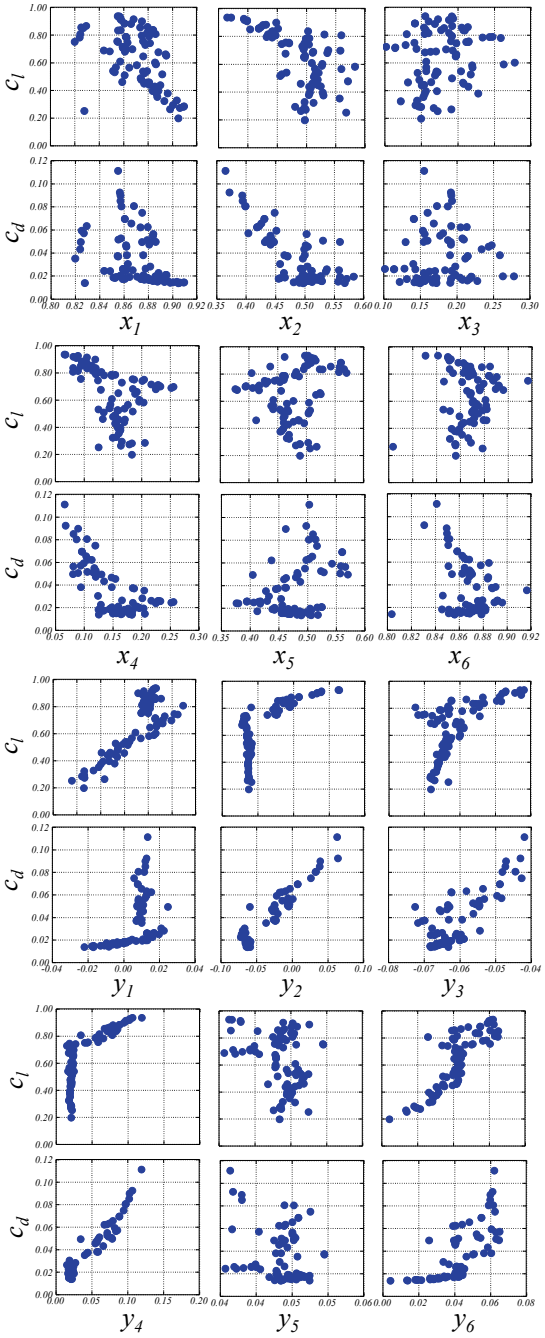

Fig. 12. Scatter plot matrix of the design parameters with respect to the lift or drag coefficients.

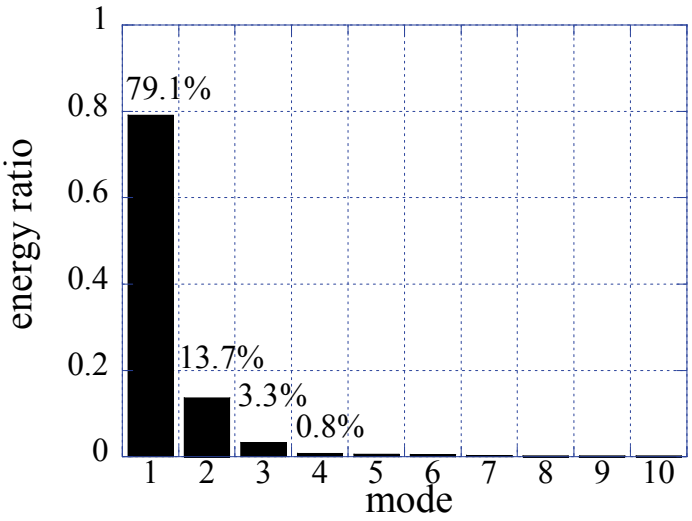

Fig. 13. Energy ratio of the top 10 principal modes of the pressure field distribution.

Figure 14 plots the components of the eigenvector of the first four modes with respect to the index of the non-dominated solutions (left) and the lift coefficient (right). This figure indicates that the pressure field of the non-dominated solutions can be categorized into three groups as the result of the shape data mining, namely, low-drag designs ($1 \le n \le 39$), high-lift-to-drag-ratio designs ($40 \le n \le 52$), and high-lift designs ($53 \le n \le 85$). Among the low-drag designs, the components of the first and second modes increase monotonically to zero as n or C_l (n) increases. Among the high-lift-to-drag-ratio designs, the first mode increases monotonically as n or C_l (n) increases, whereas the second mode is approximately

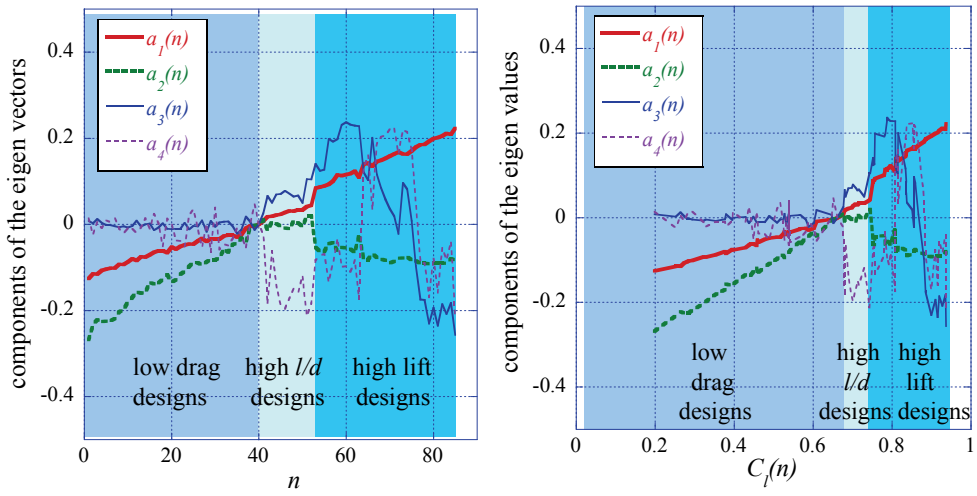

Fig. 14. Eigenvectors of the first four modes of the pressure field distribution.

zero. Among the high-lift designs, the first mode increases monotonically as n or C_l (n) increases, whereas the second mode decreases monotonically as n or C_l (n) increases. In this figure, a large jump in the components of the eigenvectors is also observed between n = 52 and n = 53. This jump indicates a significant change in the flow field between the high-lift-to-drag-ratio designs and high-lift designs.

The orthogonal base vectors of the first and second modes are shown in Fig. 15. These vectors indicate that the major changes among the pressure fields of the non-dominated solutions are 1) on the lower surface side near the trailing edge (region 1), 2) on the lower surface side near the leading edge (region 2), and 3) on the upper surface (region 3). These vectors also indicate that the pressure on the lower surface side near the leading and trailing edges decreases as the pressure on the upper surface side decreases.

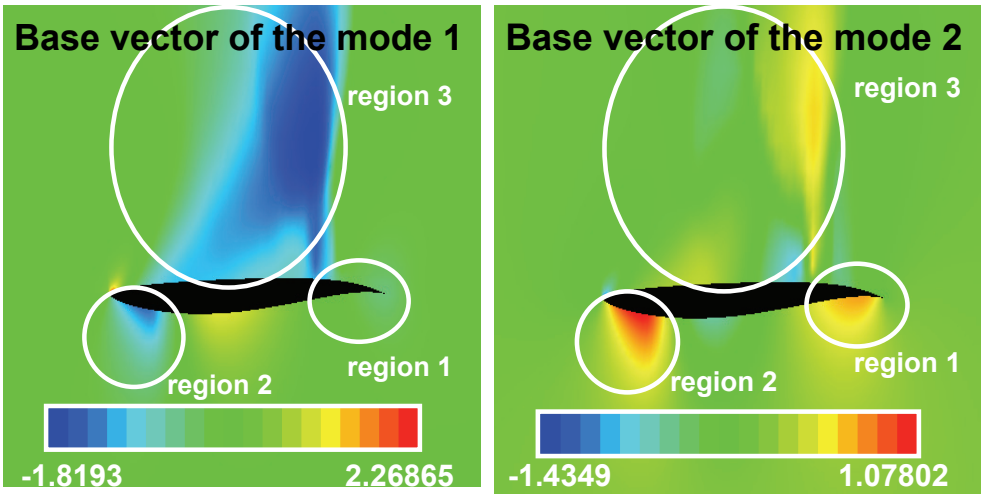

Fig. 15. Orthogonal base vectors of the first and second modes of the pressure field.

Recalling that the pressure fields of the non-dominated solutions are represented by Eqs. (1) and (2) and that the first and second modes are dominant (more than 92%), the eigenvectors (Fig. 14) and base vectors (Fig. 15) of the first and second modes and the pressure field of the maximum-lift-to-drag-ratio design (Fig. 16) provide the following observations:

1. In region 1, the second mode is dominant because the base vector of the first mode is approximately zero. Since the base vector of the second mode in region 1 is positive, the eigenvector of the second mode indicates that the high-lift-to-drag-ratio designs have the highest pressure near the trailing edge on the lower surface and that the pressure in region 1 increases monotonically as n (or lift) increases among the low-drag designs.
2. In region 2, the base vector of the first mode is negative, whereas that of the second mode is positive. The absolute value of the second mode is approximately half that of the first mode. Among the low-drag designs, the eigenvectors of the first and second modes increases monotonically as n (or lift) increases, and the absolute value of the second mode is approximately double that of the first mode. These facts indicate that the pressure field in region 2 does not change much among the low-drag designs because the first and second modes cancel out. Among the high-lift-to-drag-ratio

designs, the eigenvector of the first mode increases monotonically, whereas that of the second mode is approximately zero, which indicates that pressure in this region decreases as n (or lift) increases. Among the high-lift designs, the pressure in this region decreases drastically as n (or lift) increases.

3. In region 3, as in region 2, the pressure field does not change much among the low-drag designs because the first and second modes (the first and second terms of the right-hand side of Eq. (2)) approximately cancel out. Among the high-lift-to-drag-ratio designs and high-lift designs, the pressure in region 3 increases as n (or lift) increases. The jump in the components of the eigenvectors of the first and second modes is due to strong shock wave generation on the upper surface.

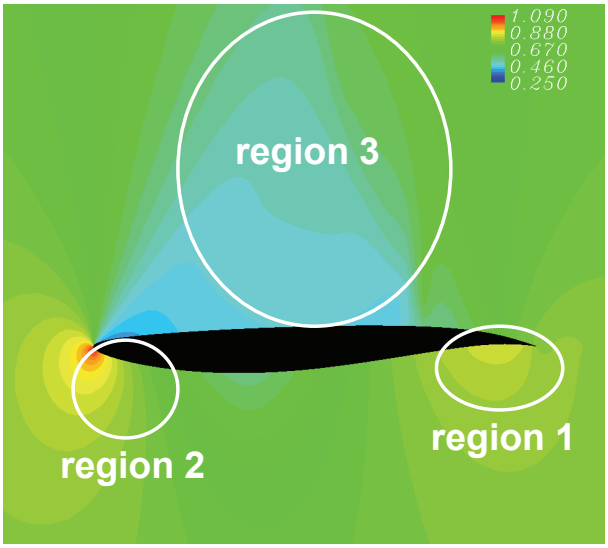

Fig. 16. Pressure field of the maximum-lift-to-drag-ratio design

7. Conclusion

A new approach for knowledge extraction from large data set of the non-dominated solutions is presented and applied to the non-dominated solutions of an aerodynamic transonic airfoil shape optimization. This approach decomposes the data of all non-dominated solutions into principal modes and base vectors using POD. One can discover knowledge from large data set of the non-dominated solutions by analysing the principal modes and base vectors. One of the advantages of this method is that the knowledge one can obtain does not depend on how the shape is parameterized for design optimization. Another advantage is that data mining of flow data leads to understanding of the physics behind the design problem.

This chapter demonstrated knowledge extraction from shape and static pressure data of non-dominated solutions of an aerodynamic transonic airfoil shape design optimization problem. The present result showed feasibility and benefit of data mining of such data.

Though the application of the POD-based data mining method was limited to the non-dominated solutions of a two-objective aerodynamic shape optimization problem in this

chapter, its application is not limited to two-objective aerodynamic optimization problems. Application of this method to design optimization problem in other research field such as structure and heat transfer is straightforward. Application to non-dominated solution of a three or more objective design optimization problem is also possible if it is coupled with other visualization methods and/or data mining methods such as scatter plot matrix and SOM. The POD-based data mining method has strong potential for innovation in design in space engineering.

8. Acknowledgements

The present research is supported in part by KAKENHI (20760552) and KAKENHI (20246122).

9. References

Baldwin, B. S. & Lomax, H. (1985). Thin-Layer Approximation and Algebraic Model for Separated Turbulent Flows, *Proceedings of the 16th Aerospace Sciences Meeting*, 78-257, Huntsville, Alabama, January 1978, American Institute of Aeronautics and Astronautics, Reston, Virginia

Brant, A. (1977). Multi-Level Adaptive Solutions to Boundary Value Problems. *Mathematics of Computation*, Vol. 31, No. 138, 333-390, ISSN 0025-5718

Chiba, K.; Oyama, A.; Obayashi, S. & Nakahashi, K. (2007a). Multidisciplinary Design Optimization and Data Mining for Transonic Regional-Jet Wing. *Journal of Aircraft*, Vol. 44, No. 4, 110-1112, ISSN 0021-8669

Chiba, K. & Obayashi, S. (2007b). Data Mining for Multidisciplinary Design Space of Regional-Jet Wing. *Journal of Aerospace Computing, Information, and Communication*, Vol. 4, No. 11, 1019-1036, ISSN 1542-9423

Deb, K. (2001). *Multiobjective Optimization Using Evolutionary Algorithms*, John Wiley & Sons, Ltd., ISBN 047187339X, Chichester, UK

Donald, R. J.; Matthias, S. & William, J. W. (1998). Efficient Global Optimization of Expensive Black-Box Function. *Journal of Global Optimization*, Vol. 13, 455-492, ISSN 0925-5001

Eshelman, L. J. & Schaffer, J. D. (1993). Real-Coded Genetic Algorithms and Interval Schemata, In: *Foundations of Genetic Algorithms 2*, Whitley, L. D., (Ed.), 187-202, Morgan Kaufmann Publishers, Inc., ISBN 1558602631, San Mateo, CA

Fonseca, C. M. & Fleming, P. J. (1993). Genetic Algorithms for Multiobjective Optimization: Formulation, Discussion and Generalization, *Proceedings of the 5th International Conference on Genetic Algorithms*, pp. 416-423, ISBN 1-55860-299-2, Champaign, Illinois, July 1993, Morgan Kaufmann Publishers, Inc., San Mateo

Goldberg, D. E. & Richardson, J. (1987). Genetic Algorithms with Sharing for Multimodal Function Optimization, *Proceedings of the Second International Conference on Genetic Algorithms*, pp. 41-49, ISBN 0-8058-0158-8, Cambridge, Massachusetts, October 1987, Lawrence Erlbaum Associates, Inc., Mahwah

Goldberg, D. E. (1989). *Genetic Algorithms in Search, Optimization and Machine Learning*, Addison-Wesley Publishing Company, Inc., ISBN 0201157675, Reading, MA

Kanazaki, M.; Tanaka, K.; Jeong, S. & Yamamoto, K. (2007). Multi-Objective Aerodynamic Exploration of Elements' Setting for High-Lift Airfoil Using Kriging Model. *Journal of Aircraft*, Vol.44, No.3, 858-864, ISSN 0021-8669

Kohonen, T. (1998). *Self-Organizing Maps, 2nd edition*, Springer, ISBN 3540679219, Heidelberg, Germany

Obayashi, S. & Wada, Y. (1994). Practical Formulation of a Positively Conservative Scheme. *AIAA Journal*, Vol. 32, No. 5, 1093-1095, ISSN 0001-1452

Obayashi, S. & Guruswamy, G. P. (1995). Convergence Acceleration of an Aeroelastic Navier-Stokes Solver. *AIAA Journal*, Vol. 33, No. 6, 1134-1141, ISSN 0001-1452

Obayashi, S.; Sasaki, D. & Oyama, A. (2004). Finding Tradeoffs by Using Multiobjective Optimization Algorithms. *Transactions of the Japanese Society for Aeronautical and Space Sciences*, Vol. 27, 51-58, ISSN 0549-3811

Obayashi, S.; Jeong, S. & Chiba, K. (2005). Multi-Objective Design Exploration for Aerodynamic Configurations, *Proceedings of the 35th AIAA Fluid Dynamics Conference and Exhibit*, CD-ROM, Toronto, Ontario, June 2005, AIAA, Reston, Virginia

Obayashi, S. & Chiba, K. (2008). Knowledge Discovery for Flyback-Booster Aerodynamic Wing Using Data Mining. *Journal of Spacecraft and Rockets*, Vol. 45, No. 5, 975-987, ISSN 0022-4650

Oyama, A. & Liou, M. S. (2002). Multiobjective Optimization of Rocket Engine Pumps Using Evolutionary Algorithm. *Journal of Propulsion and Power*, Vol. 18, No. 3, 528-535, ISSN 0748-4658

Oyama, A.; Shimoyama, K. & Fujii, K. (2007). New Constraint-Handling Method for Multi-objective Multi-Constraint Evolutionary Optimization. *Transactions of the Japan Society for Aeronautical and Space Sciences,* Vol. 50, No. 167, 56-62, ISSN 0549-3811

Oyama, A.; Okabe, Y.; Shimoyama, K. and Fujii, K. (2009). Aerodynamic Multiobjective Design Exploration of a Flapping Airfoil Using a Navier-Stokes Solver. *Journal of Aerospace Computing, Information, and Communication*, Vol. 6, No. 3, 256-270, ISSN 1542-9423

Oyama, A.; Kawakatsu, Y. & Hagiwara, K. (2010). Application of Multiobjective Design Exploration to SOLAR-C Orbit Design, Proceedings of the 20th workshop on JAXA Astrodynamics and Flight Mechanics, Sagamihara, Japan, July 2010, ISAS/JAXA, Sagamihara (to be appeared)

Shimoyama, K.; Lim, J. N.; Jeong, S.; Obayashi, S. & Koishi, M. (2009). Practical Implementation of Robust Design Assisted by Response Surface Approximation and Visual Data-Mining. Journal of Mechanical Design, Vol.131, No.6, 061007-1-11, ISSN 1050-0472

Sirovich, L. (1987). Turbulence and Dynamics of Coherent Structures Part 1: Coherent Structures. *Quarterly of Applied Mathematics*, Vol. 45, No. 3, 561-571, ISSN 1552-4485

Tani, N.; Oyama, A. & Yamanishi, N. (2008). Multiobjective Design Optimization of Rocket Engine Turbopump Turbine, *Proceedings of the 5th International Spacecraft Propulsion Conference* (CDROM)